

CEWES MSRC/PET TR/98-17

# Structure Significant Representation of Structured Datasets

by

Raghu Machiraju

Zhifan Zhu

Bryan Fry

Robert Moorhead

**DoD HPC Modernization Program**

Programming Environment and Training

**CEWES MSRC**



**Work funded by the DoD High Performance Computing  
Modernization Program CEWES  
Major Shared Resource Center through**

Programming Environment and Training (PET)

Supported by Contract Number: DAHC 94-96-C0002  
Nichols Research Corporation

Views, opinions, and/or findings contained in this report are those of the author(s) and should not be construed as an official Department of Defense Position, policy, or decision unless so designated by other official documentation.

# Structure Significant Representation of Structured Datasets

Raghu Machiraju<sup>1,3</sup>, Zhifan Zhu<sup>4</sup>, Bryan Fry<sup>2,3</sup>, Robert Moorhead<sup>2,3</sup>

<sup>1</sup>Department of Computer Science

<sup>2</sup>Department of Electrical and Computer Engineering  
Mississippi State University, Mississippi

<sup>3</sup>NSF Eng. Res. Center for Computational Field Simulation

<sup>4</sup>Duke Engineering, Las Vegas, NV

## Abstract

Numerical simulation of physical phenomena is now an accepted way of scientific inquiry. However, the field is still evolving with a profusion of new solution and grid generation techniques being continuously proposed. Concurrent and retrospective visualization are being used to validate the results, compare them among themselves and with experimental data, and browse through large scientific databases. There exists a need for representation schemes which allow access of structures in an increasing order of smoothness (or decreasing order of significance). We describe our methods on datasets obtained from curvilinear grids. Our target application required visualization of a computational simulation performed on a very remote supercomputer. Since no grid adaptation was performed, it was not deemed necessary to simplify or compress the grid. In essence, we treat the solution as if it were in the computational domain. Inherent to the identification of significant structures is determining the location of the scale coherent structures and assigning saliency values to them [22][23]. Scale coherent structures are obtained as result of combining across scales the coefficients of a wavelet transform. The result of this operation is a correlation mask that delineates regions containing significant structures. A spatial subdivision (e.g., octree) is used to delineate regions of interest. The mask values in these sub-divided regions are used as a measure of information content. Later, another wavelet transform is conducted within each sub-divided region and the coefficients are sorted based on a perceptual function with bandpass characteristics. This allows for ranking of structures based on the order of significance, giving rise to an adaptive and embedded representation scheme. We demonstrate our methods on two datasets from computational field simulations. Essentially we show how our methods allow the ranked access of significant structures. We also compare our adaptive representation scheme with a fixed blocksize scheme.

CR Categories and Subject Descriptors: I.3.2 [Computer Graphics]: Graphics Systems; I.3.8 [Computer Graphics]: Applications; I.4.2 [Image Processing]: Compression (Coding).

**Additional Keywords:** wavelet transform, structure detection,

human visual system, progressive transmission

## 1 INTRODUCTION

Given the advances in hardware and the proliferation of new numerical and data analysis techniques, the solution grids for computational simulations are continuously becoming larger. For instance, even 100 time steps using a grid size of  $69 \times 43 \times 15$  from a computational field simulation (CFS) requires the storage of the computational grid, a vector field (velocity) and two scalar fields (density, energy), all in floating point format, making the storage requirement 136 Mbytes. Both *concurrent* and *retrospective* visualization are employed to understand the results of a simulation. The size of the datasets is a burden, especially when they are transmitted over a slow network. It is not uncommon that the domain for a simulation is spatially divided into several zones and executed on a multicomputer or a cluster of networked processors. Each zone has its own geometric grid and a designated processor, or solver. Visualizing the solution data from the solvers in real-time or near-real-time provides instantaneous feedback and therefore allows tracking of the simulation. Such systems are becoming increasingly available [9][20]. In this case, visualization is done in a distributed manner, i.e., the solution data are transferred from the solvers to a graphics workstation over the network and selectively visualized. Therefore, it is useful for the datasets to be stored and transmitted in a compressed format. Even more important for solutions which have not converged yet is a quick meaningful preview so that the simulation can be steered.

A coarse-to-fine progressive display is often used. However, it may be useful to display the most significant structures first. In Fig. 1 we show an iso-surface rendering of pressure around a turbine. The structures are ranked in terms of singularity; it is useful to see structure A in its entirety before structure D which is far smoother. It is easier to gauge the shape of D than of A and hence a coarser rendition of D is sufficient. The structures are displayed again in Fig. 1b using a rate (percentage of complete information) of 20%. The structure A is faithfully rendered while structure D is quite distorted. The *embedded visualization* paradigm allows a ranking of

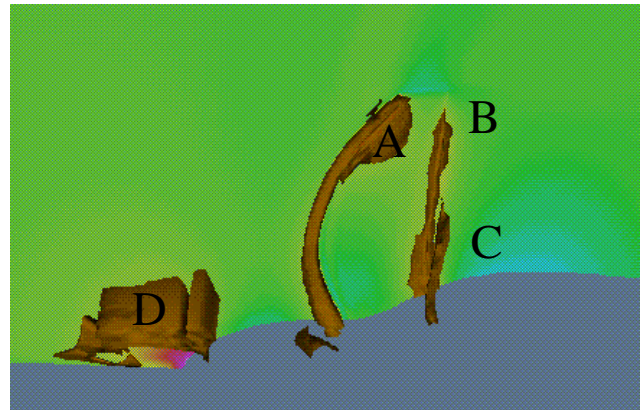
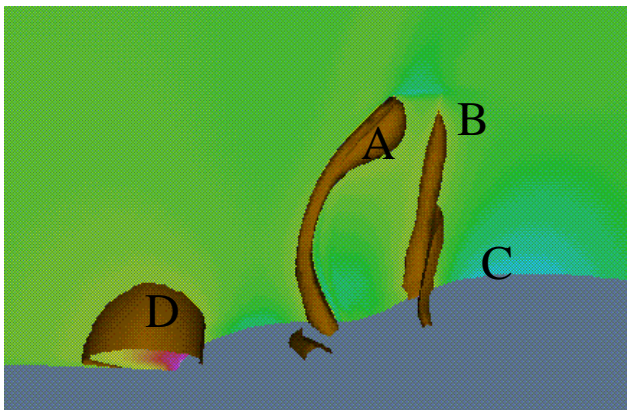


Figure 1. Structure Significant Visualization: (left) Iso-surface rendering of pressure around a turbine is depicted. The structures A, B, C, and D are ordered in terms of increasing smoothness. (right) Iso-surfaces rendered with only 20% of wavelet coefficients.

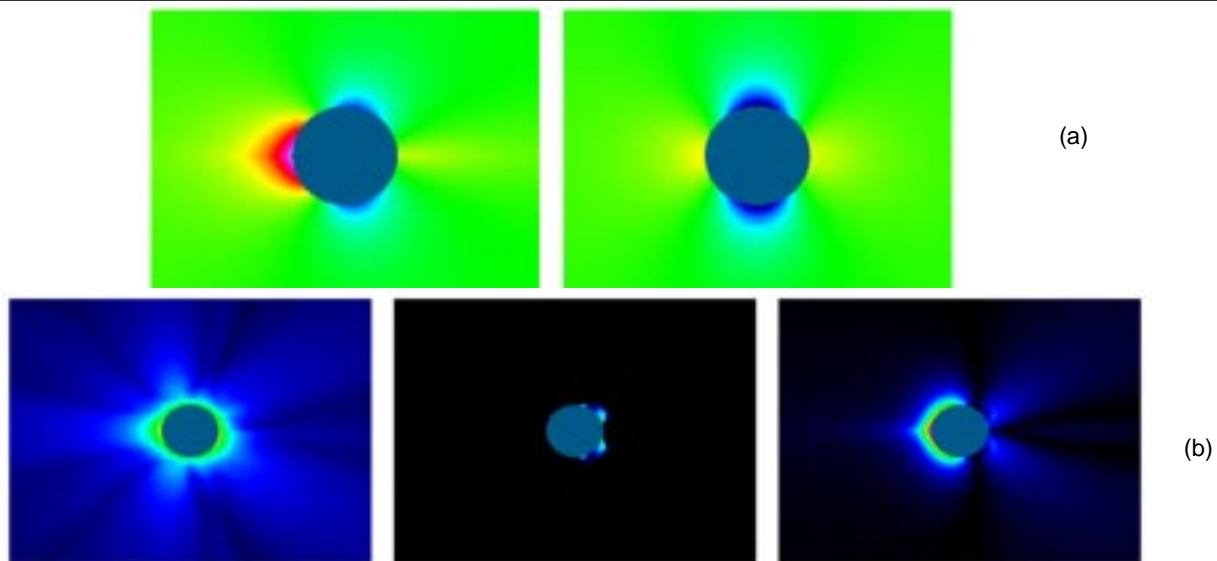


Figure 2. (a) Density around a right circular cylinder computed using first (left) and second order (right) upwind methods. (b) Density computed around an airfoil at 0 (left), 1 (middle), and 4 (right) degree angles of attack. (Courtesy: John West, DoD Major Shared Resource Center, US Army Corps of Engineers, Vicksburg, MS.)

structures and can be very useful for concurrent visualization. This paradigm of visualization is different from displaying a progressively smoother version of the complete rendering. We believe that progressive refinement is less useful for scientific visualization. Given the loss of detail in the subsampled images, features cannot be easily discerned. A computational scientist cannot learn much about the physical phenomenon from a subsampled image. Also, it is not clear that the bandwidth is efficiently utilized.

The needs for retrospective visualization are equally stringent. Given the increased use of computational methods to solve engineering and scientific problems, large archival collections of datasets now exist and terascale visualization is no longer a concept but a need for scientists working on large-scale problem. There is a need therefore to index, browse and retrieve through a scientific database. The indexing can be in the form of a coarse-to-fine structures, while browsing and retrieval require the display of structures as described in Fig. 1. Also, computational scientists often need to compare the results of a simulation with another (Fig. 2; same physical condition with different solver) and with experimental data. Thus, methods which allow side-by-side comparison of datasets based on the structures will be useful. Even more useful will be a method which will display progressively refined structures based on some parameter like rate. Once again, an embedded scheme can be employed to enormous benefit. Transform coding schemes have been used for efficient transmission and compressed storage of images. The discrete cosine transform and the wavelet transform have been used for this purpose. Both lossy and lossless schemes have been used to store and transmit datasets. The new paradigm of visualization proposed here can also be supported by the same transform coding and multi-resolution framework.

We now examine some characteristics of CFS datasets which require special consideration when designing representation schemes:

- CFS datasets are generally very sparse, since the computational experiment attempts to study and focus on very specific phenomenon and sometimes at very specific locations in the domain. Most of the information is packed in a very small portion of the entire volume irrespective of the grid topology used.
- CFS datasets sometimes have sharp singularities like a shock. However, as Fig. 2 shows the singularities are not very sharp and a method like edge detection will fail to detect regions of activity. Wavelet methods on the other hand are often able to locate the significant structures.
- For computational field simulations it is important that any representation be inherently lossless. However, it is also imperative that the compression scheme allow for selective display of important structures in a dataset.
- Finally, CFS datasets come in a variety of shapes and sizes, often dictated by the underlying geometry and the desired resolution of structures. Many multiresolutional schemes impose *power-of-2* restrictions on the resolution. A commonly used solution is padding the dataset until *power-of-two* resolutions are obtained. This increases the quantity of data that must be transmitted, sometimes significantly. Thus, it may be worthwhile to partition the dataset into blocks wherein the wavelet transform can be applied.

**Proposed Method** - To satisfy all our requirements of concurrent and retrospective visualization, we make use of a technique which identifies regions of significant structures in datasets. The structures we locate are scale coherent, i.e., contain all frequencies across scales. Our method is two-pass in nature. In the first pass, a spatial subdivision is obtained which delineates regions of high spatial frequency. The subdivision is obtained by creating a correlation mask from the wavelet transform. This step may require temporary padding of the volume to create power-of-two dimensions. An octree embedding of this mask provides the required subdivision. In the second phase each block of the partition is coded separately using an appropriate function from a wavelet library. This step does not require any padding of the original volume. Later, the wavelet coefficients in each of the blocks are sorted and packed based on the presence of significant structures. The visual content associated with coefficients within each block is estimated by employing a computational model of the Human Visual System (HVS). The final result is an embedded encoding of the

volume, wherein a ranking of coefficients is possible. Our multi-resolution representation scheme can be very easily extended to lossy or lossless coding. Similarly, it allows for:

- browsing of datasets allowing selective and embedded display
- comparative visualization of datasets
- lossy/lossless compression of floating point data
- progressive transmission, allowing the user to stop transmission at any desired time

Our attention to the problem arose when some scientists were executing computational programs on a supercomputer at a very remote site and viewing the results on workstations. The computational problem was the study of hydrodynamics around submarine hulls (dataset 2). A structured curvilinear grid was employed to model the domain around the submarine. Given the very slow link (17 kilobytes per second) and the availability of a supercomputer it seemed imperative to employ a representation scheme that was amenable to efficient bandwidth utilization and provided useful visualization. Useful implementation on a slow link is achieved when the most important information is transmitted first. The grid was sent separately or was already known *a priori* at each end of the link. It was only the actual solution that had to be compressed for this particular situation. In essence, we treat the solution as if it were in the computational domain. Certainly this method will not apply to unstructured meshes. This approach of not including the grid geometry is far from very ideal, especially if grid simplification is the desired goal. On the other hand, simplification entails the elimination of certain grid cells and will require resampling. In computational simulations unless the grid is adapted to the solution at various epochs, it is perhaps moot or even incorrect to simplify the grid. Convergence of the solution is often a very difficult task and uncontrolled simplification can destroy the integrity of the solution.

In Section 2 we motivate the need for a variable block sized multiresolution representation and review past reported methods in volume compression. In Section 3 we present our scheme for multiresolution volume representation and in Section 4 we present our embedded progressive transmission scheme which allows a perceptual ranking of structures. Results are presented in Section 5 and in Section 6 we draw conclusions and discuss future work.

## 2 BACKGROUND

In this section we describe the coding and analysis capabilities of the wavelet transform. Later, we describe a particular computational model of the human visual system. Our proposed method includes this model to perceptually rank structures in a dataset. The words signal, image, and volume are used synonymously in this paper. Also the words compression and coding are employed to describe a representational technique.

Previous volume compression methods include predictive methods [11], fractal methods [3], vector quantization (VQ) [28], DCT [42], wavelets [9][13][26][27][32][34][38][39][40], and gaussian pyramids [12]. The predictive method (followed by Huffman coding) reported in [11] provided sufficient improvement over the standard UNIX utilities like *gzip*, but did not provide a high level of compression. Also, it was not amenable to embedded coding for progressive transmission. Ning and Hesselink [28] used VQ to compress volume data and achieved a high level of compression. However, the method is again not very amenable to concurrent progressive transmission given the asymmetric nature of the coder and decoder. The coding effort is generally orders of magnitude higher than expended in the decoding component. The fractal technique

of [3] is expensive and is not amenable to progressive transmission. Among the transform coding methods the DCT, wavelet, Gaussian and Laplacian image pyramids have found common use. However, the work reported in both [12] and [42] emphasizes less the compression aspect and more the rendering of images from the compressed domain. There exist other methods which have been borrowed from image coding and are suitable for hardware implementation [19].

We now describe multiresolution representation schemes based on wavelets. Our focus is on schemes which are (a) adaptive, (b) embedded, and (c) assign perceptual saliency and hence ranking to structures when employed in conjunction with a simple computational model of the HVS. Such schemes will allow one to achieve the goals of efficient concurrent and retrospective visualization. Adaptive methods which are adept at capturing higher order smooth (beyond edges) singularities and can locally adjust in terms of spatial resolutions can provide more efficient representation schemes.

**First Generation Wavelet Representations** - In transform Coding (TC) methods the image or volume is projected to a transformed space spanned by adequate basis functions. The goal of all TC methods is to de-correlate the signal and scale the energy in the projected space so that a few coefficients can adequately represent the signal. The wavelet transform has gained much popularity due to some very attractive properties including compact support of the basis functions and the ability to represent functions of arbitrary smoothness [6]. Analysis and compression can be obtained by retaining only a portion of the coefficients. The size of the retained portion is dictated by the desired quality of the resulting image or the smoothness of the function. It has been shown in [8] that an image can be suitably represented by the first  $N$  coefficients within a certain error tolerance measured in spaces spanned by smooth functions. Methods which retain only  $N$  coefficients are often classified as *first generation methods* [9][13][26][32][34][38]; they do not attempt to characterize the behavior from the sub-band information. Rather, they apply standard and computationally viable techniques for compression and transmission.

**Second-Generation Wavelet Representations** - As pointed out in [10], second generation methods are driven by structures in an image. Moreover, it is essential that a human observer or a model of the HVS be included in the coding scheme. These methods attempt to locate information in an image and then proceed with coding the coefficients which exist in the identified areas. Much information in an image is concentrated in a few regions. These are dominated by structures characterized by discontinuities in intensity and manifest as edges (images) and boundaries (volumes). Mallat and Zhong [25] used spline wavelets to obtain a redundant wavelet decomposition. The end result of their non-orthogonal transform is a hierarchy of local absolute maximas and hence multiscale edges. These maximas are not searched for; instead a numerical procedure is used to characterize the Lipschitz coefficients of singularities. Westermann [39] implemented the same ideas to detect structures in a time-varying 3D volume. Edge-based methods suffer from the disadvantage of being error prone in the presence of noise or when the image has a profusion of small features or texture. A significant method, wavelet probing, was presented in [5] to segment the image into smooth regions which are coded very efficiently. The identified edge regions are then coded separately by employing the same technique. Although the method may yield high coding efficiency, it does not facilitate the rankings of structures as described in Fig. 1. The proposed method fits in this same category.

**Adaptive Methods:** Adaptive methods which are adept at capturing higher order smooth (beyond edges) singularities and

can locally adjust in terms of spatial resolutions can provide more efficient representation schemes. A compression and progressive transmission scheme for visualization should maximize the information presented while minimizing the data rate. This objective can be explained by using an information-rate curve. If the information in a data volume is uniformly distributed over the data domain and the bit budget is uniformly allocated for each point, this curve will be linear. In most cases, however, the information contained in a dataset is non-uniformly distributed, resulting in a non-linear curve. The desired information-rate curve should have a sharp rise as close to the zero-rate as possible, so that most of the data information can be visualized as early as possible. This is a departure from the rate-distortion perspective normally espoused in the image coding literature. To achieve the requirements of concurrent and retrospective visualization an embedded scheme can be used, where the information is ranked by perceptual significance and transmitted accordingly over the channel [32][43]. In [30] a zerotree wavelet structure is created from the wavelet space. This allows for a grouping of wavelet coefficients of similar significance in a hierarchical fashion and facilitates an embedded representation that is well suited for progressive transmission. In [18] this technique was expanded to include a computational model of the HVS. Said and Perlman extended this algorithm and obtained superior results [29].

Since the wavelet transform is performed using a single mother wavelet, the transform is essentially signal independent. To adapt to the statistical properties of the data, wavelet packet techniques [4] decompose the signal by choosing from a library of wavelet packets the wavelets that best represent the signal. However, the computational expense is still staggering and the wavelet packet transform is far from robust. An aspect of the wavelet packet transform can be usefully employed; spatial subdivision of the image is conducted and normally a quad/octree is used in conjunction with the subdivision of the frequency bands. Each block of the spatial subdivision can be coded with a different wavelet basis, the choice being dictated by a variety of reasons including measures of function smoothness.

Thus, we have described the basic rationale for our method and outlined the methodology. Two essential elements are missing, namely a technique to detect structures and a description of a computational model of the HVS. We describe a methodology in Section 3 for detecting structures across scales and end this section with a description of the Contrast Sensitivity Function (CSF) and a computational model of the HVS.

**Human Visual System (HVS)** - The human cortex is often modeled as a linear system and its response to a visual excitation in the receptive field is expressed as a convolution of the impulse response of the visual cortex with the input stimulus. Equivalently, the response to an input can be obtained by multiplying the Contrast Sensitivity Function (CSF) with the Fourier transform of the input. The CSF measures the response of the visual system to different frequencies. It is important to note that the response is lower for higher frequencies. Attempts have been made to measure the CSF of the human visual system. For instance, Mannos and Sakrison [21], after conducting a series of psychophysical experiments on human subjects, found that the CSF can be modeled by the function in Equation 1 (Fig. 3a). Here,  $f_s$  is spatial frequency in cycles per degree.

$$C_s(f) = [0.0492 + 0.2964 f_s] e^{-(0.114 f_s)^{1.1}} \quad (1)$$

A 2D (or a 3D) version can be easily obtained and is shown in Fig. 3b. The discrete orthogonal wavelet transform does not serve as a computational model for the HVS. To include the CSF into our

methods, a frequency decomposition induced by a dyadic wavelet transform is imposed on the CSF (Fig. 3a). Thus, for each band a weight can be computed which is then applied to the wavelet transform. The coefficients at each level and location are modulated using a perceptual weight obtained by integrating the CSF over the area occupied by the band in a 3D frequency space. Fig. 3a shows the CSF function mapped to image frequency and the superimposed wavelet transform subdivision in 1D. Thus, after  $m$  levels of the wavelet transform the weight is given as:

$$C_m = \frac{\left( \int_{FB_m} C_s(\omega) d\omega \right)}{A(FB_m)} \quad (2)$$

where  $FB_m$  is the frequency subband  $\left( \frac{\pi}{2^m}, \frac{\pi}{2^{m-1}} \right)$  in question

and  $A(FB_m)$  is the width of the band. The weights are precomputed and stored in a table. In Fig. 7b we report the normalized weights for a 2D subdivision [18]. The weights are based on the assumption that the image is viewed at a distance six times the image height. In the following section we show how structures can be adaptively detected.

### 3 ADAPTIVE STRUCTURE DETECTION

The volume representation scheme reported herein has the four components shown in Fig. 4. The block representation allows for the ranking and measurement of important information in a signal. The progressive transmission scheme requires another component to order the blocks (Section 4). The first three components facilitate the detection of significant structures while the fourth component achieves the actual coding. We now describe each component in detail.

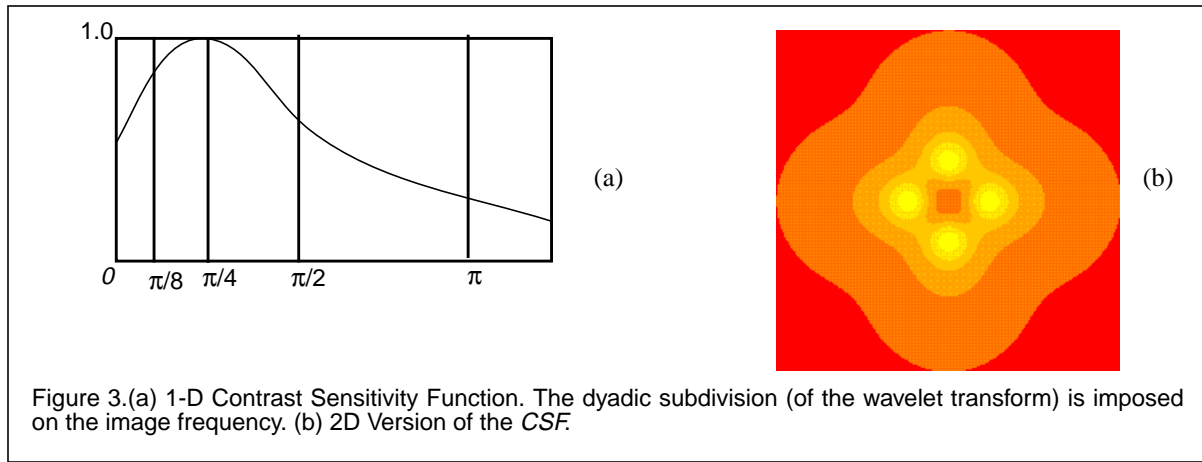
**Wavelet Transforms** - We used both the dyadic wavelet transform and the non-orthogonal wavelet transform of Mallat and Zhong [25]. The biorthogonal wavelet transform is employed to code the image in each block. The choice of the non-orthogonal transform allows for a better characterization of the local spatial frequencies of the underlying function. Moreover, it does not suffer from the aliasing problems that the critically sampled dyadic transform suffers from. The result of the wavelet transform is a pyramid of detail subvolumes and a smooth subvolume. The subband volumes are of the same size as the original volume.

In [35] a study of different biorthogonal wavelets for coding efficiency was conducted. Our choice of the second wavelet was dictated by that study. We chose the biorthogonal filter of second order since it provides adequate results. The reported method should work for any volume at any resolution. However, its effectiveness depends on the partitioning of the volume into regions which are then coded individually. Padding is required for resolutions which are not powers-of-two for the first wavelet transform. Once the partition is obtained the padded regions are discarded and only the original volume is considered. More details on the wavelet transform can be found in much reported work including [6][24]. It now remains to identify the coefficients which contribute to structures in an image. We now provide some motivation of our basic structure detection method. More details can be found in [22][23].

#### 3.1 Wavelets As An Analysis Tool

The wavelet transform provides valuable information for the *space-frequency* diagram or the *scalogram* [6][15]. A space-fre-





quency diagram describes the frequency content of the image at a pixel location at different scales of resolution. The impulse and the infinitely long sinusoidal wave are extreme examples. The space-frequency diagram for the impulse signal is defined at only one instance in the space domain (localized) while it completely occupies the frequency range (not localized). The situation is changed when the sinusoidal signal is considered. Only one location of the frequency spectrum is occupied (localization) while the signal persists over all points in space. We now informally describe the shape of the space-frequency diagram of any signal. We derive it from the shape of a corresponding diagram of an impulse.

**Space-frequency Diagram Of An Arbitrary Signal-** The wavelet transform of a *Delta Dirac* function  $\delta$  centered at  $x=0$  with respect to a wavelet function  $\psi$  is given as:

$$W[\delta; \psi](a, b) = \frac{1}{a} \psi\left(\frac{b}{a}\right) \quad (3)$$

The space frequency diagram ( $a$  - scale parameter;  $b$  - time/space parameter), thus, has all frequencies. The set of points in the half plane forms the so-called *cone-of-influence* (Fig. 5a). Now consider a function composed of the sum of  $n$  deltas located at  $x=x_n$ , each scaled differently by a factor  $k_n$ . From the property of linearity [15] of the wavelet transform we get

$$W[f_n; \psi](a, b) = \sum_n k_n \frac{1}{a} \psi\left(\frac{b-x_n}{a}\right) \quad (4)$$

The cone-of-influence is now shown in Fig. 5b. The cone is shifted towards the smaller scales such that the bottom is outside the half plane. Since all signals can be expressed as the summation of infinitely many *Dirac* functions, it can be said that the wavelet transform of all signals has a shifted cone form. It is our goal to determine the intersection of the cone with the x-axis. The significant structures populate only this spatial region. The rest of this section describes the process of locating them and assigning saliency to them.

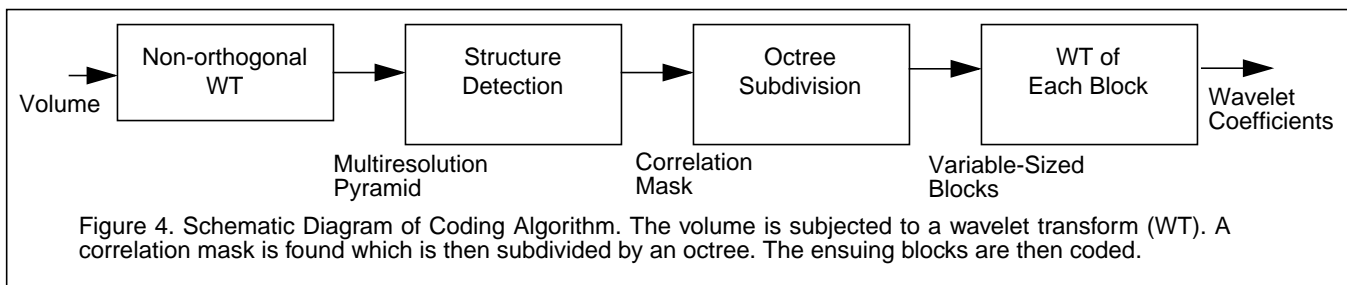
**Combining Function** - The combining function  $C$  is defined as follows [22][23]. For a  $J$ -level wavelet decomposition  $W$ , at all  $x$ ,  $C$  exists and is given by

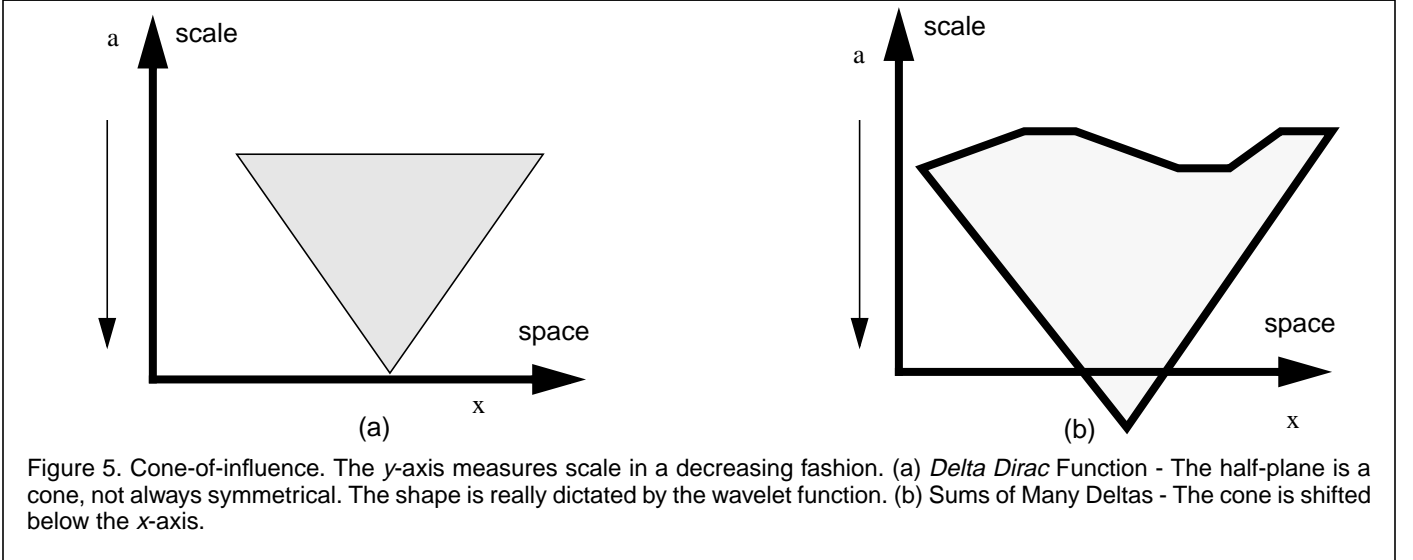
$$C(x, J, W) = |A_J(x)| \prod_{j=1}^J |D_j(x)| \quad (5)$$

where  $A_j$  and  $D_j$ ,  $j = 1 \dots J$ , are the sub-band functions at location  $x$ . Thus, we obtain a floating point mask which has the same size as the image. We now state some observations about the mask and discuss scale-coherent structures.

**Scale Coherent Structures** -  $C(x, J, W) = 0$  implies the absence of structures at that location. This arises from the cone-like shape of the wavelet transform. Where  $C(x, J, W) > 0$  coherent structures exist and lie within the support of the cone. The effectiveness of the method presented in this paper rests on the following observations:

- As  $J$  becomes large and approaches infinity (if possible), the result of the combining function should approach the support of the continuous wavelet transform. The idea behind the combining function is simple. The smallest scales have the smallest supports and hence by multiplying across scales one obtains a size equal to the size of the smallest support. Similar observations and arguments were made for images elsewhere [1].
- It is possible that a non-dyadic powers-of-two transform will yield a better mask since the space-frequency diagram is measured at a large number of scale positions. Thus, a more accurate mask can be obtained if an  $M$ -band ( $M > 2$ ) spectral subdivision is conducted.
- In Fig. 6 we show the effect of combining. The masks in Fig. 6b and Fig. 6c have been greatly exaggerated for display purposes. The former is obtained through the use of the orthogonal transform while the latter is obtained from the application of the non-orthog-





onal transform of [25]. The mask in Fig. 6c is smoother. The masks are from two different yet nearby locations which contain similar structures. The product is high at locations near the point of discontinuities. The product locates correlated structures across scales. The number of scales, the size of the structures, and the wavelet functions used also contribute to the effectiveness of the combining algorithm.

- Noise reduction occurs in the product. Un-correlated additive noise in the spatial domain becomes correlated in the wavelet domain [15]. However, the size of the correlation is smaller in the coarser scales. Thus, in the smooth space measured by  $A_j$ , un-correlated noise is suppressed and the coefficients arising from the noise process measure close to zero.
- If  $f$  is Lipschitz ( $\alpha$ ), the function  $f$  is defined as

$$|f(x) - P_n(x)| \leq Kx^\alpha \quad n \leq \alpha \leq n+1$$

Essentially, the function  $f$  differs from a  $n$ -degree polynomial by a bounded oscillatory fraction. All known practical functions are known to satisfy this definition of a Lipschitz function. The wavelet coefficients at level  $j$  are bounded [17] as shown:

$$|W[f](j, x)| \leq K2^{j\alpha} \quad (6)$$

The combining function is then bounded by

$$C(x, J, W) \leq A^{S(J)} 2^{\alpha S(J)}, \quad S(J) = \sum_{j=1}^J j \quad (7)$$

where the function  $S(J)$  is the sum of the positive integers up to  $J$ . Other functions may be used instead of the product. The logarithm may also be employed. In that case the combining function is bounded as

$$\log(C(x, J, W)) \leq S(J) \log A + \alpha S(J) \quad (8)$$

Since the mask depends on the value of  $\alpha$ , the value of the mask is an indication of the significance of the singularity. Larger values of  $\alpha$  indicate presence of significant singularities. Hence the above arguments for the effectiveness of the mask in capturing singularities are valid.

### 3.2 Scale-Coherent Structure Detection

Edge detection captures all the zero crossings of the second derivative of a function; a mask delineates all high frequency regions. If the wavelet had a regularity of *one* then the combining mask would contain mostly edges. Our method employs simple strategies to combine information across scales and is rooted in the approximation theory perspective of the wavelet transform [15]. Starck et al. [31] report a combining method which employs the sum of binary thresholded wavelet coefficients to create a mask. The binarization process loses important detail and can introduce blockiness. We, however, explore the use of the product function. The product of the wavelet transform is a more natural choice since it arises from the shape of the wavelet transform. The location of structures and the assignment of saliency values is, therefore, more accurate. Xu et al. independently developed an algorithm based on the product [41]. Their motivation was based on the fact that correlation of structures is best captured by the product. Also, they attempt to find edges rather than regions of arbitrary singularity. Our motivation stems from the detection of structures, and denoising is a component in the process. By using the product of the wavelet transform, we obtain a mask which identifies the location of structures and assigns them saliencies. The wavelet transform of the image and its inverse transform form the first and last stages of the algorithm, respectively. The other components of the algorithm extract a minimal possible representation of the image in terms of coherent structures.

**Denoising** - CFS datasets are not tainted with as much noise as those from medical scanners are. Uncertainty arising from computational inaccuracies, number representations (truncation, overflow, and underflow), and grid tolerances does exist. The ensuing noise can be suitably modeled with a Gaussian distribution function. This characterization although not paramount to the functioning of many numerical schemes does allow for better location of features. As described in Section 4, the process of combining inherently denoises. It is, however, useful to denoise even before generating the sub-band mask. That way we have a minimum number of coefficients that go into the construction of the mask. We resort to the statistical thresholding methods of Donohoe and



Johnstone [7]. We implement an adaptive thresholding scheme which determines the threshold at different levels from a noise model.

**Feature Based Thresholding** - More coefficients can be eliminated based on the relative magnitude of the product mask. A typical discriminating function shown in Equation 10 is employed to remove insignificant features and to shrink the dynamic range. We describe the equation for images. The quantity  $C(i,j)$  is the mask value at pixel  $(i,j)$ ,  $C_{max}$  is the maximum value of the mask,  $g$  is a tunable parameter, and  $R$  is the current dynamic range. The value of  $g$  controls the number of structures (and hence coefficients). Values between 1.1 and 1.5 have been found to be acceptable for most images. Higher values of  $g$  degrade the visual quality of the image.

$$d = R \times \log \left( 1 + \left( \frac{C(i,j)}{C_{max}} \right)^g \right) / \log(2) \quad (9)$$

Wherever the sub-band mask is set to zero, the corresponding coefficients in the pyramid have to be set to zero. In other words, the sub-band mask has to be propagated back into the multiresolution pyramid. As a result of this thresholding operation, only the coefficients contributing to coherent features remain. Since, the subband images are the same size as the original image, the thresholding becomes trivial.

### 3.3 Octree Subdivision of the Mask

The spatial subdivision allows the identification of coherent regions in the image. Several options exist including region growing and recursive spatial decomposition methods. Region growing algorithms are not very amenable to user control and can result in blocks of odd shape and size. Hence we resort to recursive spatial subdivision methods based on quad/octrees. The level of the tree is controlled by the user thus producing square/cubic blocks. Otherwise, a crude homogeneity measure can be employed to control the subdivision process. A threshold measuring the amount of information is used. The subdivision process stops when the amount of information is small as measured by the user threshold. Thus, a larger threshold would yield larger blocks. We show the spatial subdivision obtained using a slice of the data in Fig. 6d. There will be some blocks which do not carry any information; they arise in the proximity of the discontinuities. The effectiveness of the adaptive partitioning scheme is made evident in Section 5 when the performance is compared against fixed block partitioning schemes. In the following section we describe how the wavelet coefficients in the blocks can be packed for progressive transmission, i.e., our embedded representation scheme.

## 4 RANKING OF STRUCTURES

In this section we describe the packing of data for progressive transmission. The blocks obtained from the spatial subdivision of the mask are sorted based on the information content within each block. A single bitstream is created from the wavelet transform coefficients of the partitioned blocks for transmission or storage. The rationale behind this scheme is to insert the most vital information at the beginning of the bitstream. Such a scheme then allows for transmission until the desired target rate is achieved. The information content can be measured in a variety of ways including the mean-square error. However, the MSE is not a viable measure of saliency in an image [33]. Rather, a weighted MSE based on perceptual considerations is gaining much popularity and is being used in image coding extensively [37]. The resulting bitstream is constructed from coefficients obtained from blocks in an order

determined by the presence of significant structures.

We employ a 3D version of the CSF to code a given volume. In reality, there is no physical justification for such a function. However, it is not uncommon to employ modulation transfer functions (MTF) to alter the significance of coefficients in a transformed space. Thus, we can conceivably construct a device which accentuates frequencies in the central portion of a 3D spectrum. To avoid unnecessary confusion we, however, use the terms CSF and MTF synonymously. The perceptual weighting of wavelet coefficients is commonly done in the image coding literature. The modulation with a perceptual function allows one to give some bands higher weights. Thus, if an inverse wavelet transform is performed and a visualization is performed, the structures which are perceptually significant are enhanced while the less significant ones are subdued. The pertinent visualization technique can influence perception of the phenomenon. However, a choice and ranking of structures based on perceptual significance does not impair the perceptual abilities of the viewer.

In reality we need a function which allows us to rank the coefficients. It seemed convenient to use the perceptual function. Our weighting scheme is an approximate one. The perception modulation function should be applied to the images; however, we apply it early on in the visualization pipeline. In the case of parallel projection the application of the 3D function is not improper. In reality the 3D function is a simple extension of a 2D function; a parallel projection will only alter a scaling factor but not the essential characteristics of this function. We now show how the perceptual weight can be incorporated into a packing scheme.

**Perceptual Weighted Embedded Packing Scheme** - The following scheme is designed to select the next significant coefficient based on the structure information estimated in each block. As a result a wavelet coefficient bitstream is constructed with the coefficients carrying the most information being placed in the stream as early as possible. After data partitioning, the data volume is represented by  $N$  variable-size blocks,  $B_i$ ,  $0 \leq i \leq N$ . Each block  $B_i$  has the following entities:

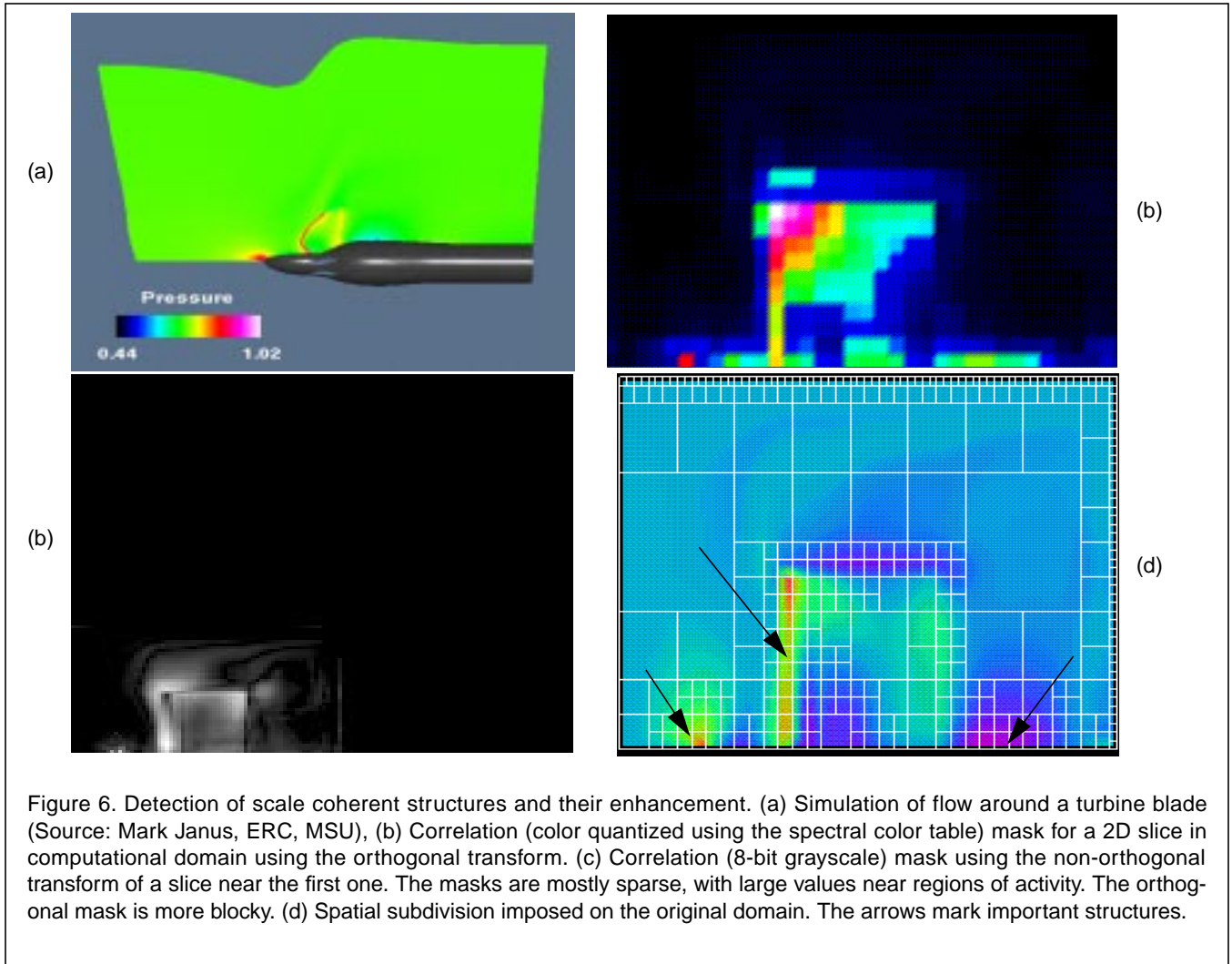
- The starting spatial address  $(i,j,k)$  and the block size.
- The information quantity contained in the block,  $H_i$ , which is defined as the sum of all correlation mask values contained in the block.
- The wavelet coefficients computed for the data block.

The measurement of the information in a block does not have to be exact. As long as  $H_i$  is a monotonic function it will suffice. Since the mask is created from the product and non-linearly enhanced with a logarithm function,  $H_i$  will be monotonic. Blocks of the same size will have the same CSF weight but different  $H_i$ s. Thus the visual significance of a wavelet coefficient is a relative quantity and is determined by two factors:

- the quantity of information in the block to which the wavelet coefficient belongs, namely  $H_i$
- the position of the wavelet coefficient inside the block.

During embedding, the relative significance of the blocks and coefficients has to be constantly updated. To do so, we calculate for each block  $RH_i$ , the remaining information, using a CSF which is pre-computed for each possible block size. This function should have the following properties:

$$\begin{aligned} RH_i(N_i) &= 1 \\ RH_i(0) &= 0 \end{aligned} \quad (10)$$



where  $N_i$  is the number of coefficients in a block.

Thus, a  $2k \times 2k \times 2k$  block will have  $8k^3$  coefficients, each measuring the information available in a subband. In the case of a 2-level, 2D wavelet transform, the dyadic decomposition results in the subdivision shown in Fig. 7. Each band in the dyadic decomposition is pre-computed and assigned a value, i.e., each position in the block  $(i,j,k)$  is assigned a normalized weight  $NCSF(i,j,k)$  (prefix  $N$  indicating normalization). A possible candidate for the function  $RH$  is

$$RH_i(m) = H_i \left( 1 - \sum_{m \in Embedded} NCSF(i, j, k) \right) \quad (11)$$

The function  $RH$  essentially computes the perceptual information that can still be assigned to the block after  $m$  coefficients have been embedded. When a coefficient is embedded in the bitstream the corresponding normalized weight is subtracted from the value of  $RH$ . The coefficients inside a block are selected in a zig-zag order similar to the selection scheme in JPEG [36]. Once a coefficient is embedded, the corresponding perceptual weight is subtracted. This scheme distinguishes between blocks that have the same spatial dimension but different information content. Given our octree spatial subdivision of the original domain, several such similar sized blocks can exist, some with little information. The

packing algorithm can be summarized as follows:

Step 1: Sort the blocks in descending order, using  $H_i$  as the key.

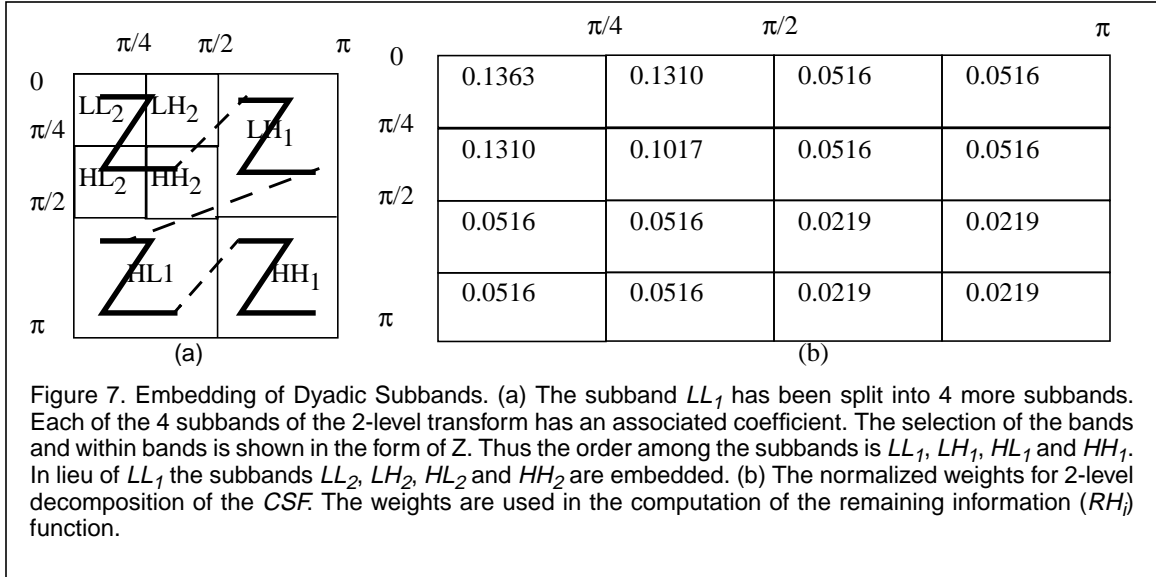
Step 2: Insert into the bitstream the lowest subband coefficient for each block and update  $RH_i$  accordingly. Re-sort the blocks based on  $RH_i$ .

Step 3: Insert into the bitstream coefficients (determined by the Z patterns) from the first block in the sequence and update  $RH_i$  until the first block is no longer the most significant block.

Step 4: Insert-sort the first block into the block sequence based on  $RH_i$ ; go back to Step 3. In [29][30] a variant of this embedded packing scheme is described.

The block addresses and the ordering information must be coded and stored precisely first in the bitstream. This can be done either by:

- coding the block addresses in the ordered sequence, or



- creating a ‘bit-volume’ and putting the block’s sequence number at the block’s reference address in the volume, and then coding the bit-volume.

We now provide the results of applying our coding scheme to a dataset from a simulation.

## 5 RESULTS

We tested our methods on 2 datasets. The first one is obtained from a simulation of the non-steady flow of fluid between turbine blades. The flow of fluid is axi-symmetric. Fig. 6a shows a slice of the density field juxtaposed with the body of the turbine [16]. The regions of interest are the leading and trailing edges of the blade and the tip of the propeller. The grid is curvilinear and is of size  $69 \times 43 \times 15$ . The solution of the simulation yielded two scalar fields (density,  $\rho$ ; energy,  $e$ ) and a vector field ( $u, v, w$ ). We do not compress the grid in this exercise, rather we restrict ourselves to the scalar fields and the components of the velocity field. Thus, the grid file and the compressed solution comprise the data that needs to be transmitted or stored. To determine the correlation mask we create a larger grid of size  $128 \times 64 \times 16$  through zero-padding. An octree subdivision of the mask provides the required blocking. Starting with the original data in each block, we then perform a wavelet transform. Finally the coefficients and the blocks are all embedded into a bitstream. The orthogonal wavelet transform was employed to obtain the embedded representation.

We selected another dataset (Fig. 9a) on which to test our technique. Since it was of mutual interest, we choose to attack concurrent visualization of an evolving flow. The volume is divided into 16 zones and horizontal symmetry is assumed so that the flow is only computed in 8 zones, 4 in the front and 4 in the back, each zone spanning a 45 degree cylindrical wedge. Each zone is of size  $81 \times 73 \times 17$ . The purpose of the simulation was to determine integrated quantities such as thrust and torque at various angles of attack. In the picture a cutting plane in the  $k$  direction ( $k=1$  for zone 1) is shown with the pressure (a derived quantity) mapped onto it. A  $i$  slicing plane at  $i=60$  in zone 1 is shown in green. A slicing plane at  $k=1$  in zone 2 is shown in red. The colormap used in all of the zone 3, timestep 2 ( $qq32$ ) data is also shown. We now discuss the rate-distortion and rate-information curves for the test datasets. The non-orthogonal wavelet transform was employed to determine the correlation mask for the second dataset.

**Rate-Distortion Curve** - The rate-distortion curve is plotted for the components of the first dataset in Fig. 8a. We define the rate to be the percent of the coefficients used. Thus a rate of one (1) would imply that all coefficients are used, while a rate of zero implies that none are used. We plot the distortion for all the fields. The distortion at a given rate is measured by finding the difference between the actual and the partially reconstructed dataset in the mean-square-error (MSE) sense. It is evident that the degradation is non-uniform over the various fields. The  $v$  and the  $w$ -component of the velocity yield similar behavior; they require that 80% of the data be used to obtain a very desirable error of 60dB. Given the axi-symmetric flow most disturbances are not in the principal flow direction. In reality, this is a very encouraging statistic. The other fields fare even better and the same distortion is obtained at the even lower rate of 20%. Essentially, the distribution of structures is very sparse and the datasets are amenable to extreme compression.

We also compared the rate-distortion performance for different partitioning schemes. The results for dataset 2 are plotted in Fig. 10. One can see that the distortion among the various quantities is more spread than in dataset 1. A reason for this observation could be the non-convergence of the solution. The adaptive schemes show more graceful degradation. The partition with higher threshold (0.5) has more desirable characteristics. The parameter  $u$  (the horizontal velocity) exhibits seemingly anomalous behavior, since the distortion is constant for the range of values plotted. A plausible explanation is that the submarine’s motion is along the same direction and thus this component of the velocity is constant. The images in Fig. 9c corroborate the rate-distortion curves.

**Information-Rate Curve** - We also plot the information that is embedded in the bitstream at different rates. The information embedded is given by the quantity  $E$ , defined as:

$$E = 1 - \frac{\sum_i RH_i}{\sum_i H_i} \quad (12)$$

Both the quantities  $H_i$  and  $RH_i$  are defined in Section 4. The denominator in the ratio measures the information content and is computed as the sum of the mask values over all the blocks. In essence it measures the information in terms of significant struc-

tures. The numerator, on the other hand, measures the information retained.

Although the rate-distortion curve is different for at least two of the components, the information-rate curve is similar for all of the parameters of dataset 1 (Fig. 8b). This is the case since we measure information in terms of structures as captured by the mask. The masks of all five components are very similar signifying that the regions of discontinuities are similar. Since the quantity  $E$  is a gross measure of perceptually significant structures in a dataset, the quantity evaluates to the same value for all components. However, the number of significant blocks is much less for the  $v$ ,  $w$  components indicating that significant structures in these datasets are much sharper or discontinuous. Thus, the rate-distortion curve is less steep and requires more coefficients to reconstruct. For dataset 2 we show the rate-information curve for the adaptive schemes (Fig. 11). The lower threshold seems to facilitate a better characterization of the information content.

**Progressive Iso-surface Rendering** - To show the efficiency of our approach we display the iso-surfaces for a derived quantity, namely pressure. We use FAST [2], a tool often used by CFS engineers to visualize their solution datasets (Note: The checker-board pattern in the background of many of the images is due to a well-known artifact of the screen door transparency rendering process used in FAST). Note that we did not take into account the uncertainty introduced by the visualization process itself. For incompressible flow, pressure at any point can be computed as follows:

$$p = (\gamma - 1) \left[ e - \frac{1}{2} \rho (u^2 + v^2 + w^2) \right] \quad (13)$$

where  $\gamma$  is a gas constant.

**Dataset 1** - For a pressure of 0.75 (the range of pressure is [0.44,1.02]) Fig. 1a shows the iso-surfaces at the full normalized rate. We see a profusion of surfaces of varying smoothness and curvature. The iso-surfaces at a rate of 20% is shown in Fig. 1b. It is again worthwhile noting that the highly curved surface in the middle is captured with high fidelity even at 20%. The smoother surface at the extreme right is captured accurately at the rate of 30% (not shown). It is important to note that even at a rate of 20% the iso-surface along the blade is captured at very high fidelity. This is a testimony to the fact that our packing scheme was effective in embedding significant structures very early in the bitstream. Another important observation is that the behavior of our scheme was not affected even though we applied our methods on a non-linear derived quantity, namely pressure. The results contained in [9] do not show the same amount of structure-sensitivity; instead the degradation at rates less than full is more uniform. In [9] CFS datasets are compressed using a non-adaptive blocking scheme.

**Dataset 2** - Since the solution has not converged there is no one correct pressure value to visualize. Thus we need to make some reasonable choice. In Fig. 9b we show the isosurfaces for pressure values of 1.3, 1.0, and 0.7. The spatial extent of the iso-surface is inversely proportional to the pressure. The pressure ranges from -1.2 to 2.6 within the volume. The small white circle is a glyph at  $i=13, j=33$  to provide some indication of the size of the isosurface plume in grid coordinates, since we do not want the shape of the isosurface to be influenced by the interpolating errors. We will use the 1.3 value for further presentation herein. The results we report are consistent for all 3 isosurface values, but only the results for pressure of 1.3 is shown for clarity.

The question naturally arises as to how much improvement is there

with the masking and variable size blocks. In Fig. 9c we demonstrate just how much. Sending only 10% of the coefficients, the isosurface for pressure of value 1.3 produces a rendition very close to that obtained when using all of the coefficients. Note that both fixed size block levels ( $4^3$  and  $8^3$ ) produce poor reproductions of the correct plume. In zones 2,4,6, and 8 there exist two low pressure regions along the body. This is shown in Fig. 12 for zone2. Note the iso-surface quality even with only 10% of the coefficients retained. The smaller isosurface at the very end of the body is visible in the lower right of each panel in Fig. 12a, near the dense nearly-vertical grid lines. In Fig. 12b is a zoomed version of the iso-surface in the low pressure region formed at the trailing end of the submarine. The glyph is at  $i=43, j=23$ , so the isosurface slices approximately  $20 \times 15$  grid cells. The colors are ordered as for the pressure field in zone 3, but the range in zone 2 is from -2.64 to -0.17.

The encoder we used is designed for testing and the timings for it are not indicative of how fast it could be. The non-optimized decoder runs in about ten seconds on an Silicon Graphics Indigo 2 with a 100 MHz R4400 CPU. Compressing floating point numbers to achieve high compression rates is not a trivial task. Usually, an entropy scheme like Huffman coding or even vector quantization can be employed to compress the wavelet coefficients [9]. It suffices to say that any further compression and quantization schemes in the wavelet domain will only enhance the efficiency of the reported scheme. The decoding cost is also small given the regular pattern of embedding the coefficients and the fact that biorthogonal wavelets were chosen to actually encode the blocks.

## 6 CONCLUSIONS AND FUTURE WORK

We presented a multiresolution representation of a volume that is amenable to high compression ratios and progressive transmission. We implemented a better method of correlation mask generation than that used in our earlier work [43]. Essentially we replaced the dyadic orthogonal transform with a non-orthogonal one. Results on two significantly different datasets are shown. Finally, we compared the performance of the adaptive partitioning methods with fixed block methods. The results obtained bear testimony to the value of the method. The method is computationally cheap and can include aspects of the Human Visual System easily. Improvements can come in the form of:

- better methods to determine the correlation mask
- better packing schemes
- adaptive choice of the wavelet function from a library

New work can include:

- further quantization of the coefficients
- detecting coherency between successive frames in a time varying simulation
- datasets from other domains (medical) and modalities
- compression of geometry

## 7 ACKNOWLEDGEMENTS

We acknowledge the contributions of Prof. Roni Yagel, The Ohio State University, and Dr. Ajeet Gaddipatti of GE Medical Systems, towards the development of the wavelet combining schemes. One of us (Raghu Machiraju) developed the schemes in

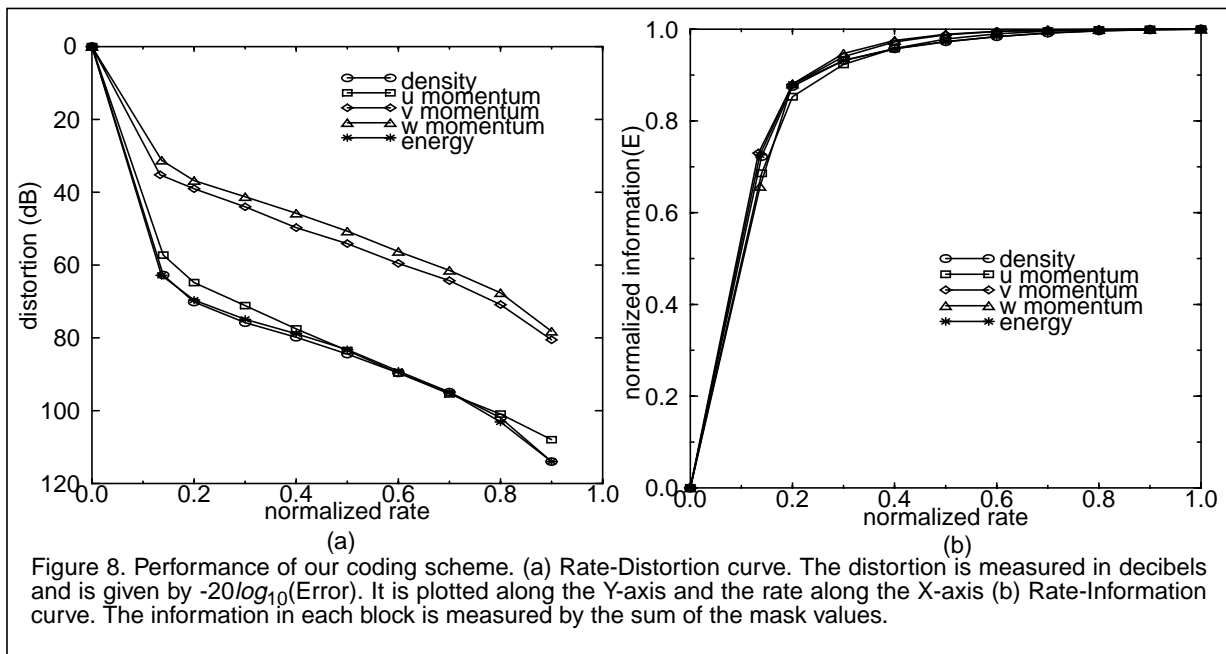


Figure 8. Performance of our coding scheme. (a) Rate-Distortion curve. The distortion is measured in decibels and is given by  $-20\log_{10}(\text{Error})$ . It is plotted along the Y-axis and the rate along the X-axis (b) Rate-Information curve. The information in each block is measured by the sum of the mask values.

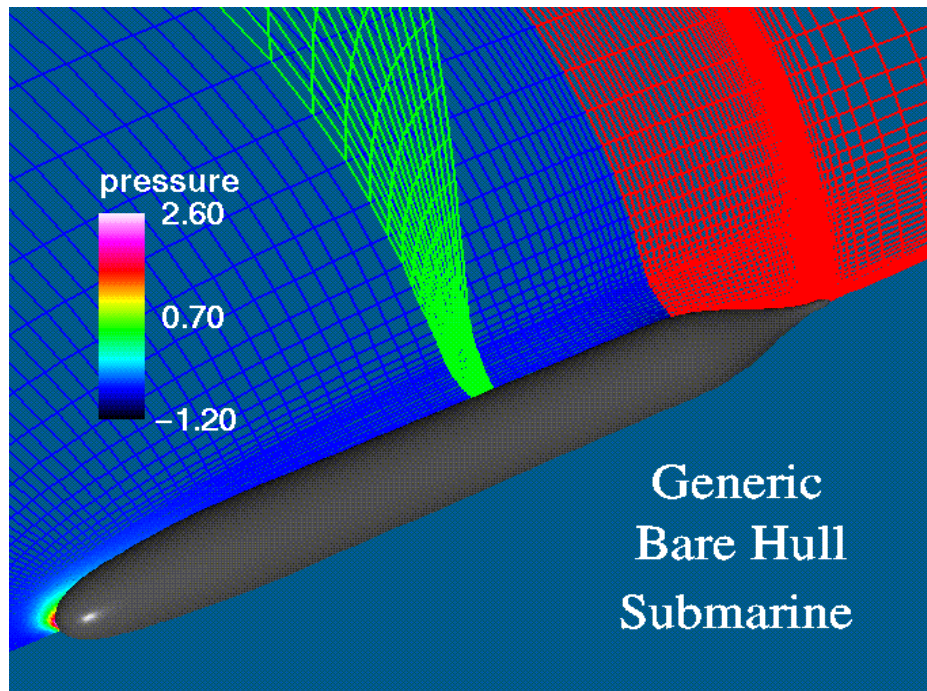
collaboration with them. This work was supported by the NSF Engineering Research Center for Computational Field Simulation, Mississippi State University and the DoD High Performance Computing Modernization Program CEWES Major Shared Resource Center through Programming Environment and Training (PET) (Supported by Contract Number: DAHC 94-96-C0002 Nichols Research Corporation). Special thanks also go to Prof. Mark Janus, Dr. Ramesh Pankajakshan, and Dr. Shyam Neerambam of the ERC for access to several datasets. One of us (Raghu Machiraju) especially acknowledges the direct support and encouragement by Prof. Joe Thompson, ERC, Mississippi State University.

## 8 REFERENCES

- [1] Antoine J.-P., Carrette P., Murenzi R., Piette B., "Image Analysis with Two-Dimensional Continuous Wavelet Transform," *Signal Processing* 31(1993):241-272.
- [2] Bancroft G., Merritt F., Plessel T., Kelaita P., McCabe R., Globus A., "FAST: A Multi-Processed Environment for Visualization of Computational Fluid Dynamics," AIAA Paper 91-0793, *Proceedings of the 29th Aerospace Sciences Meeting*, Reno, NV, January 1991.
- [3] Cochran W. O., Hart J. C., Flynn P. J., "Fractal Volume Compression," *IEEE Transactions on Visualization and Computer Graphics*, Vol. 2, No. 3, pp. 313-322, December 1996.
- [4] Coifman R. R., Wickerhauser M. V., "Entropy-Based Algorithms for Best-Basis Selection," *IEEE Transaction on Information Theory*, Vol. 38, No. 2, pp. 713-718, March 1992.
- [5] Deng B., Jawreth B., Peters G., Sweldens W., "Wavelet Probing for Compression Based Segmentation," *Wavelet Applications in Signal and Image Processing*, Editor: Laine A.F., pp. 266-276, *Proceedings SPIE* 2034, 1993.
- [6] Daubechies I., *Ten Lectures on Wavelets*, CBMS-NSF Regional Conference Series in Applied Mathematics, SIAM, Philadelphia, PA, 1992.
- [7] Donoho D. L., Johnstone I. M., "Ideal Spatial Adaptation via Wavelet Shrinkage," *Biometrika* 81:422-455, 1993.
- [8] DeVore R. A., Jawreth B., Lucier B. J., "Image Compression Through Wavelet Transform Coding," *IEEE Transactions on Information Theory*, Vol. 28, No. 2, pp. 719-746, March 1992.
- [9] Du X. S., Moorhead R. J., "Multiresolutional Visualization of Evolving Distributed Simulations Using Wavelets and MPI," *Proceedings of SPIE*, Vol. 3017, SPIE/IS&T Electronic Imaging '97, San Jose, CA, pp. 298-309, February 1997.
- [10] Froment J., Mallat S., "Second Generation Compact Image Coding with Wavelets," *Wavelets - A Tutorial in Theory and Applications*, Chui C. K. (editor), pp. 655-678, Academic Press, 1992.
- [11] Fowler J., Yagel R., "Lossless Compression of Volume Data," *Proceedings of 1994 Symposium on Volume Visualization*, Washington DC, October 1994, pp. 43-50.
- [12] Ghavamnia M. H., Yang X. D., "Direct Rendering of Laplacian Pyramid Compressed Volume Data," *Proceedings of Visualization'95*, pp. 192-199, October 1995.
- [13] Gross M., Lippert L., Dreger A., Koch R., "A New Method to Approximate the Volume Rendering Equation Using Wavelets and Piecewise Polynomials," *Computers & Graphics*, Vol. 19, No. 1, pp. 47-62, 1995.
- [14] Guo B., "A multiscale model for structure-based volume rendering," *IEEE Transactions on Visualization and Computer Graphics*, Vol. 1, No. 4, pp. 291-301, 1995.
- [15] Holschneider M., *Wavelets: An Analysis Tool*, Oxford University Press, 1995.
- [16] Janus J. M., Horstman H. Z., Whitfield D. L., "Unsteady Flow-field Simulation of Ducted Prop-Fan Configurations," AIAA-92-0521, *30th Aerospace Sciences Meeting and Exhibit*, Reno, NV, January 1992.
- [17] Jaffard S., "Wavelets and nonlinear analysis," *Wavelets: Mathematics and Applications*, Edited by J. J. Benedetto and M. W. Frazier, pp. 467-503, CRC Press, Boca Raton,
- [18] Kim Y., Cho I., Lee I., Yun T., Park K. T., "Wavelet transform image compression using human visual characteristics and tree structure with a height attribute," *Optical Engineering*, Vol. 35, No.1, pp. 204-212, January 1996.
- [19] Knittel G., "High Speed Volume Rendering Using Redundant Block Compression," *Proceeding of Visualization'95*, pp. 176-183, October 1995.
- [20] Lippert L., Gross M. H., Kurmann C., "Compression Domain Volume Rendering for Distributed Environments," *Proceedings of the Eurographics '97*, Computer Graphics Forum, Vol. 14, No. 3, 1997.
- [21] Mannos J. L., Sakrison D. J., "The Effects of a Visual Fidelity Criterion on the Encoding of Images," *IEEE Transactions on Information Theory*, 20(3):525-536, July 1974.

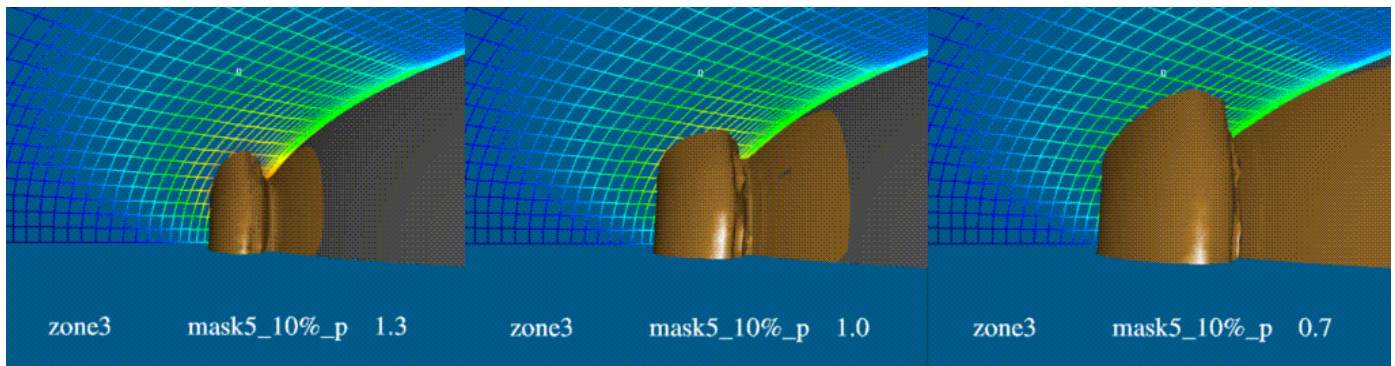
- [22] Machiraju R., "Analysis, Control and Evaluation of Image Generation in Volume Rendering," *Ph.D Thesis*, The Ohio State University, 1996.
- [23] Machiraju R., Gaddipati A., Yagel R., "Detection and Enhancement of Scale Coherent Structures Using Wavelet Transform Products," *Proceedings of the Technical Conference on Wavelets in Signal and Image Processing*, SPIE Annual Meeting, Vol. 3169, San Diego, CA, July 27 - August 2, 1997.
- [24] Mallat, S., "A Theory for Multiresolution Signal Decomposition: The Wavelet Representation," *IEEE Transactions on Pattern Analysis and Machine Intelligence*, 11(7):674-693, July 1989.
- [25] Mallat S., Zhong S., "Characterization of Signals from Multiscale Edges," *IEEE Transactions on Pattern Recognition and Machine Intelligence*, 14(7):710-732, July 1992.
- [26] Muraki S., "Volume Data and Wavelet Transform," *IEEE Computer Graphics and Applications*, Vol. 13, pp. 50-56, July 1993.
- [27] Muraki S., "Multiscale volume representation by a {DoG} wavelet," *IEEE Transactions on Visualization and Computer Graphics*, Vol. 1, No. 2, pp. 109-116, 1995.
- [28] Ning P., Hesselink L., "Vector Quantization for Volume Rendering," *Proc. of 1992 Workshop on Volume Visualization*, pp. 69-74, October 1992.
- [29] Said A., Perlman W., "A New and Efficient Image Codec Based on Set Partitioning in Hierarchical Trees," *IEEE Transactions on Circuits and Systems for Video Tech.*, Vol. 6, No. 3, June 1996, pp. 243-250.
- [30] Shapiro J. M., "Embedded Image Coding Using Zerotrees of Wavelet Coefficients," *IEEE Transactions on Signal Processing*, Vol. 41, No. 12, pp. 3445-3462, December 1993.
- [31] Starck J.-L., Murtagh F., Bijaoui A., "Multiresolution support applied to image filtering and restoration," *Graphical Models and Image Processing*, 57, pp. 420-431, 1995.
- [32] Tao H., Moorhead R., "Progressive Transmission of Scientific Data Using Biorthogonal Wavelet Transform," *Proceedings of Visualization '94*, pp. 93-99, October 1994.
- [33] Teo P., Heeger D., "Perceptual Image Distortion," *First IEEE International Conference on Image Processing*, Vol. II, pp. 982-986, November 1994.
- [34] Trott A., Moorhead R. J., McGinley J., "Wavelets Applied to Lossless Compression and Progressive Transmission of Floating Point Data in 3-D Curvilinear Grids," *Proceedings of IEEE Visualization '96*, pp. 385-388, Oct. 1996.
- [35] Vilsenar J. D., Belzer B., Liao J., "Wavelet Filter Evaluation for Image Compression," *IEEE Transactions on Image Processing*, Vol. 4, No. 8, pp. 1060-1053, August 1995.
- [36] Wallace G., "The JPEG still picture compression standard," *Communications of the ACM*, vol. 34, No. 4, pp.39-41, 1991.
- [37] Watson A. B., Gloria Y. Y., Joshua A. S., Vilsenar J., "Visual Thresholds for Wavelet Quantization Error," Human Vision and Electronic Imaging, Editors, Rogowitz B., Allebach J., *Proceedings of the SPIE*, vol. 2657, pp. 382-392, 1996.
- [38] Westermann R., "A Multiresolution Framework for Volume Rendering," *Proc. 1994 Symposium on Volume Visualization*, pp. 51-58, October 1994.
- [39] Westermann R., "Compression Domain Rendering of Time-Resolved Volume Data," *Proceedings of Visualization '95*, pp.168-175, October 1995.
- [40] Westerman R., Ertl T. "A Multiscale Approach to Integrated Volume Segmentation and Rendering," *Proceedings of Eurographics'97*, Budapest, Hungary, September 1997.
- [41] Xu Y., Weaver J. B., Healy D. M., Lu J., "Wavelet Transform Domain Filters: A Spatially Selective Noise Filtration Technique," *IEEE Transactions On Image Processing*, Vol. 3, No. 6, pp. 747-758, November 1994.
- [42] Yeo B.-L., Li B., "Volume Rendering of DCT-Based Compressed 3D Scalar Data," *IEEE Transaction on Visualization and Computer Graphics*, Vol. 1, No. 1, pp. 29-43, March 1995.
- [43] Zhu Z., Machiraju R., Fry B., Moorhead R., "Wavelet-based Multiresolutional Representation of Computational Field Simulation Datasets," *Proceedings of Visualization '97*, October 1997.



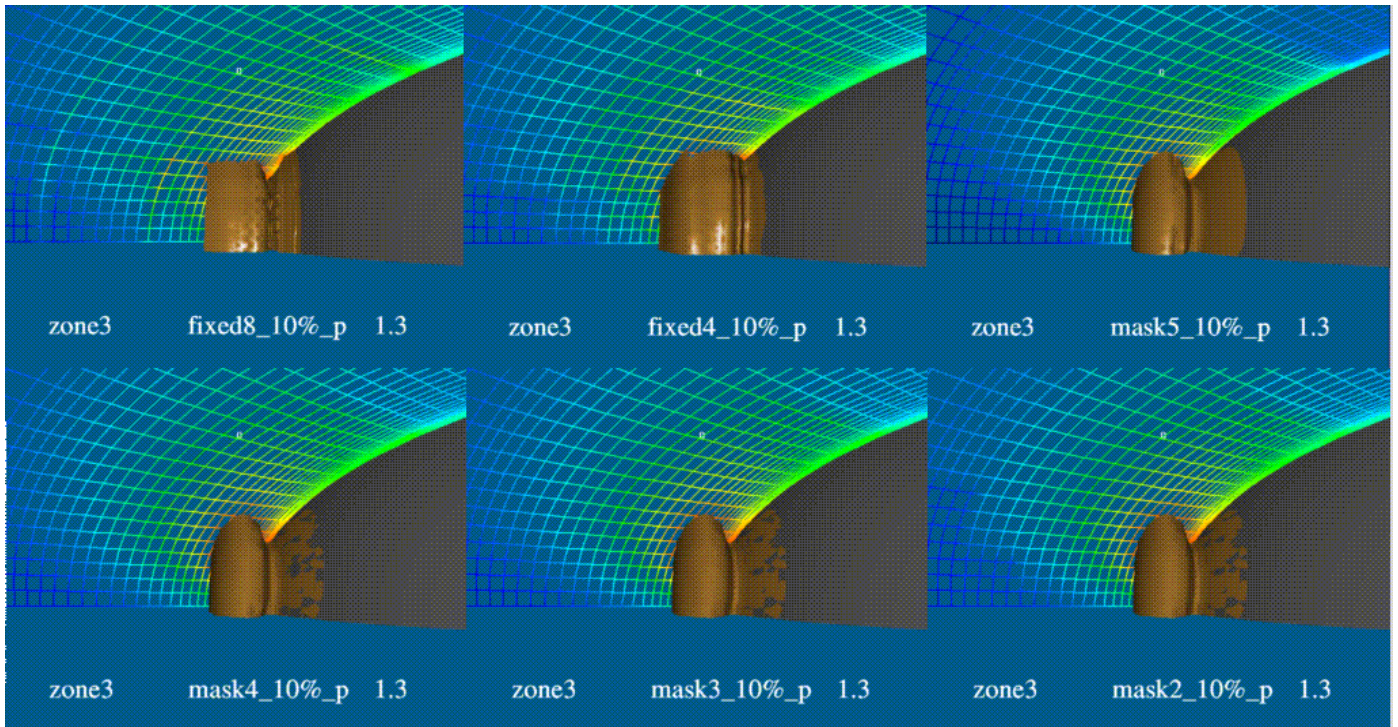


(a)

Figure 9. Flow around a submarine hull. (a) Basic configuration. The complete geometry has 8 zones, 4 in front and 4 behind. The pressure variations are shown on slice planes for various zones of the curvilinear grid. (b) For the same octree subdivision of the mask (threshold = 0.5) and rate (=10%) pressure thresholds of 1.3, 1.0 and 0.7 are visualized in zone 3 (front of submarine). (c) The efficacy of the adaptive partition is shown. The iso-surface for the pressure value of 1.3 and rate 10% is displayed for a variety of partitioning strategies. Two fixed size partitioning strategies are used. Cubes of size  $4^3$  and  $8^3$  are used and compared with partitions obtained when thresholds of 0.5, 0.4, 0.3 and 0.2 are used. It is clear that adaptive partitions are superior, especially for larger values of thresholds. Fixed partitions result in blocky iso-surfaces.



(b)



(c)

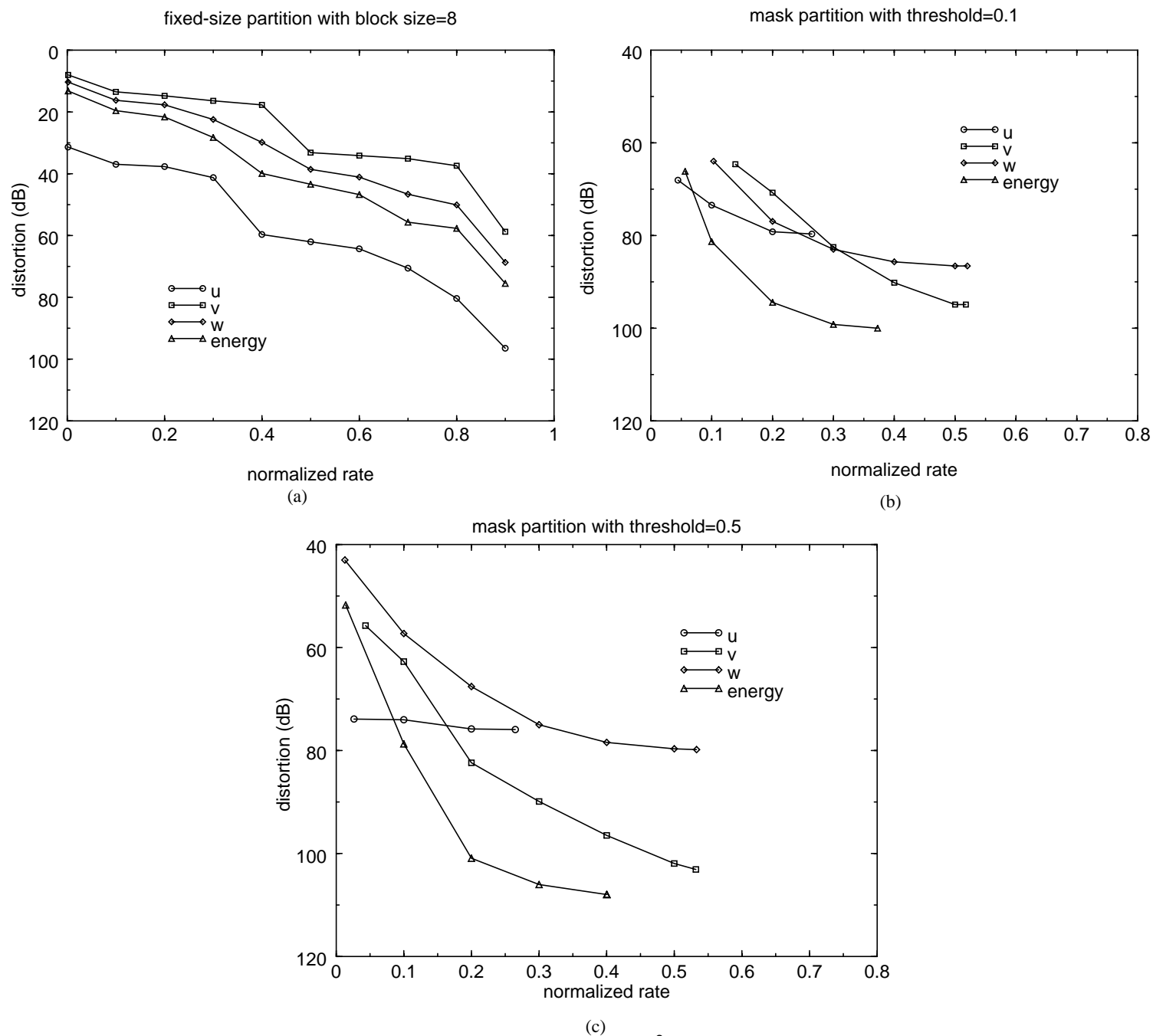


Figure 10. Rate Distortion Curves for dataset 2. (a) Fixed partition of size  $8^3$  of mask. Adaptive partition with (b) low threshold (c) high threshold.

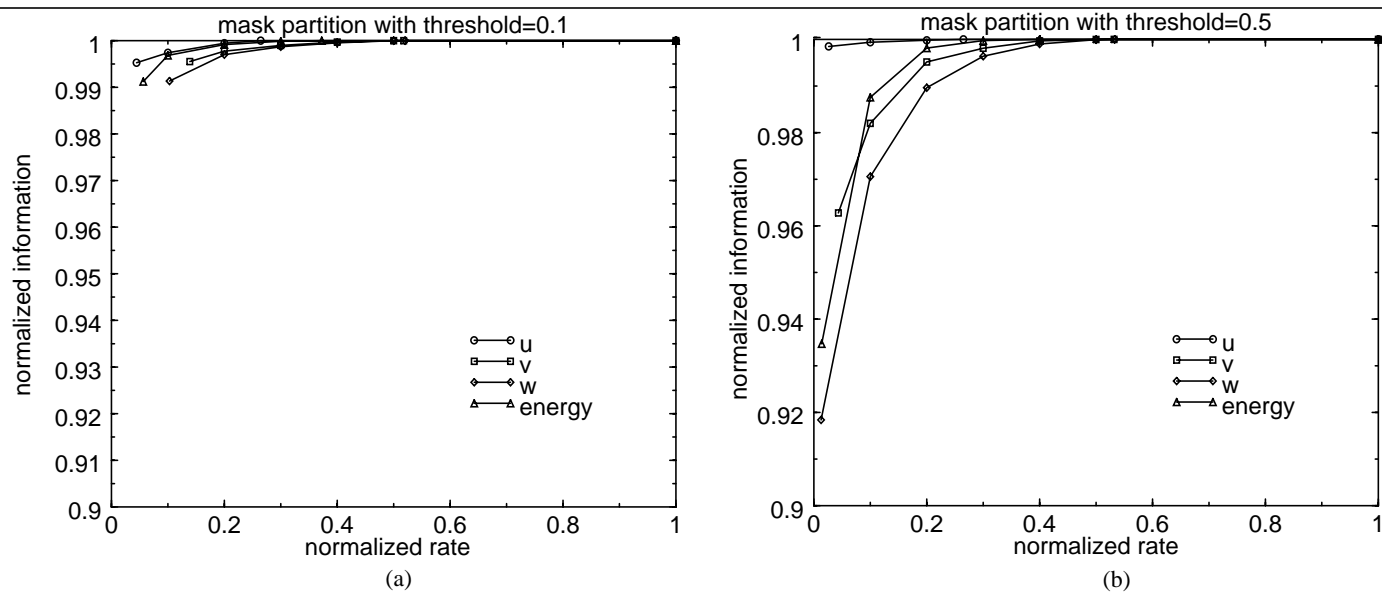
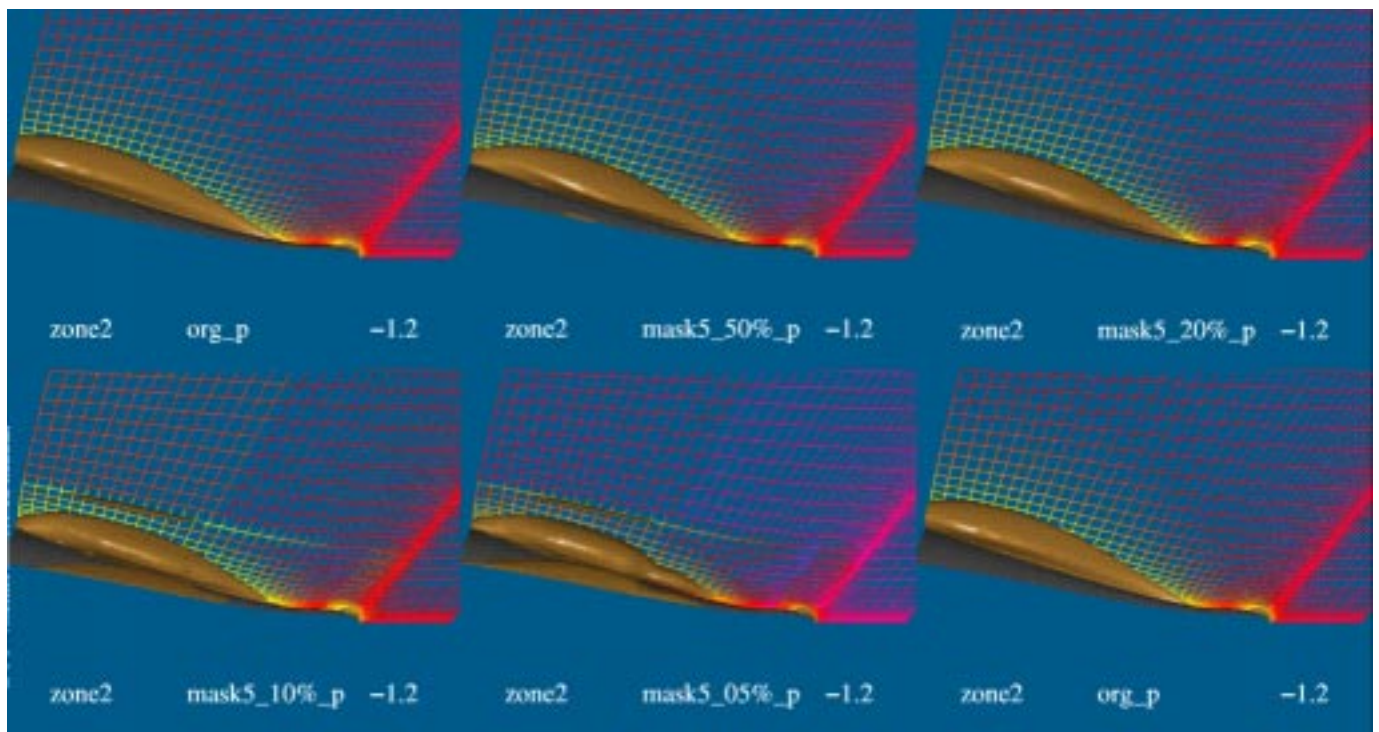
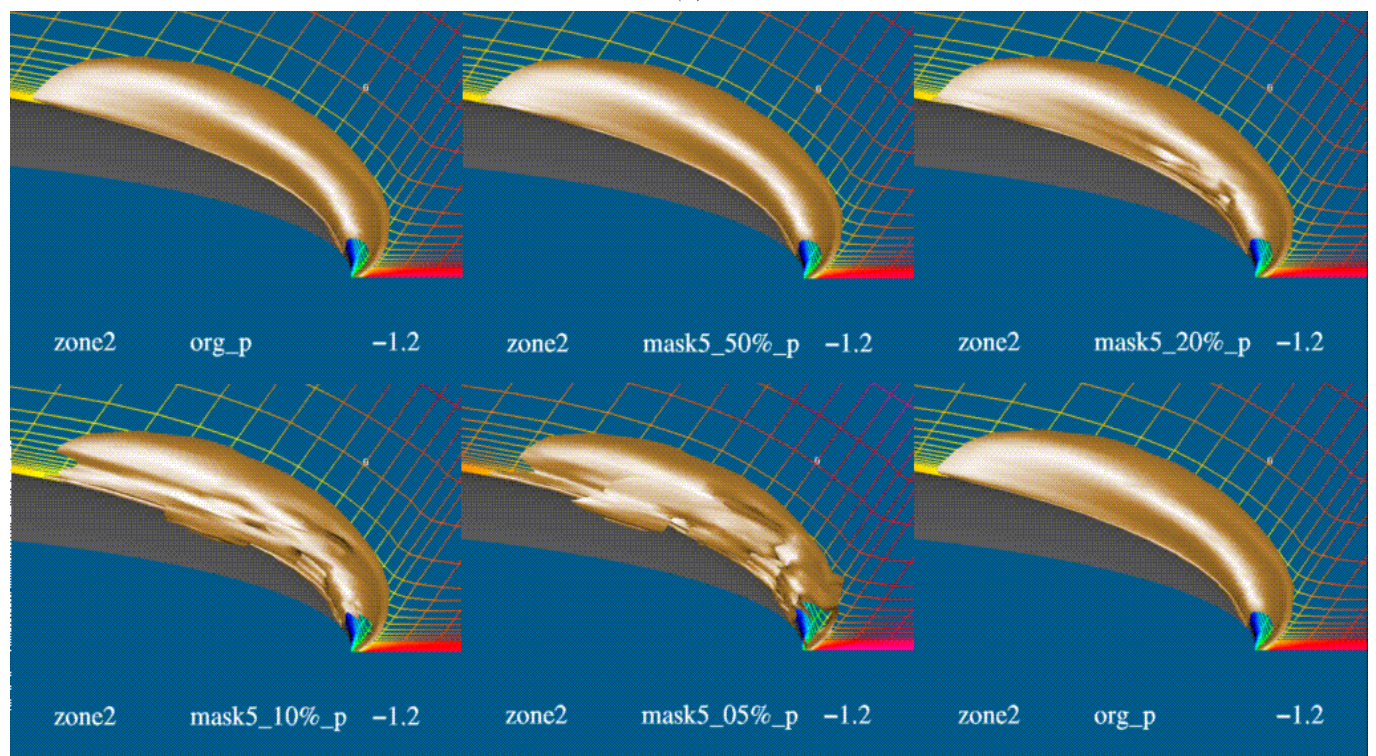


Figure 11. Information-curve performance of adaptive partitioning. (a) Threshold = 0.1 (b) Threshold = 0.5.





(a)



(b)

Figure 12. Iso-surface renderings of pressure (value = -1.2) of zone 2. (a) Different rates and same adaptive partition. (b) The lower images are zoomed versions of the above.